

# Turbulence collapses at a threshold particle loading in a dilute particle-gas suspension.

V. Kumaran,<sup>1</sup> P. Muramalla,<sup>2</sup> A. Tyagi,<sup>1</sup> and P. S. Goswami<sup>2</sup>

<sup>1</sup>*Department of Chemical Engineering,  
Indian Institute of Science, Bangalore 560 012, India.*

<sup>2</sup>*Department of Chemical Engineering,  
Indian Institute of Technology Bombay, Mumbai 400 076, India.*

## Abstract

Two mechanisms are considered responsible for the turbulence modification due to suspended particles in a turbulent gas-particle suspension. Turbulence augmentation is due to the enhancement of fluctuations by wakes behind particles, whereas turbulence attenuation is considered to result from the increased dissipation due to the particle drag. In order to examine the turbulence attenuation mechanism, Direct Numerical Simulations (DNS) of a particle-gas suspension are carried out at a Reynolds number of about 3333 based on the average gas velocity  $\bar{u}$ , channel width  $h$ , and the gas kinematic viscosity. The particle Reynolds number based on the particle diameter  $d_p$ , gas kinematic viscosity and the flow velocity  $\bar{u}$  is about 42 and the Stokes number is in the range 7 – 450. The particle volume fraction is in the range  $0 - 2 \times 10^{-3}$ , and the particle mass loading is in the range 0 – 9. As the volume fraction is increased, a discontinuous decrease in the turbulent velocity fluctuations is observed at a critical volume fraction. There is a reduction, by one order of magnitude, in the mean square fluctuating velocities in all directions and in the Reynolds stress. Though there is a modest increase in the energy dissipation due to particle drag, this increase is smaller than the decrease in the turbulent energy production; moreover, there is a decrease in the total energy dissipation rate when there is turbulence collapse. Thus, turbulence attenuation appears to be due to a disruption of the turbulence production mechanism, and not due to the increased dissipation due to the particles. There is a discontinuous collapse in the turbulence intensities at a critical particle loading, instead of the continuous decrease as the particle loading is increased.

PACS numbers: 47.55.Kf, 42.27.nd, 82.70.Kj

A central issue in the dynamics of particle-gas suspensions is the effect of the particles on the gas phase turbulence. This issue is of great physical significance in geophysical phenomena such as sandstorms and snow avalanches, as well as in industrial applications such as fluidised beds and pneumatic transport. An important question, which has been studied extensively, is whether the fluid turbulence is increased or decreased due to the presence of the particles.

When the suspended particles are in the size range  $10 - 100\mu\text{m}$ , the particle Reynolds number (ratio of fluid inertia and viscosity based on the particle diameter) is small, and so the drag force on the particles can be adequately described by the Stokes law or a modified drag law that incorporates inertial corrections. The particle Stokes number (ratio of fluid inertia and particle viscosity) is typically large. Due to this, the particles cross the fluid streamlines due to inertia, and there is a force exerted on the fluid due to the instantaneous difference in the particle and fluid velocities.

An early review by Gore and Crowe[1] reported that turbulence modification is determined by the ratio  $(d_p/L)$ , where  $d_p$  is the particle diameter and  $L$  is the integral length scale of turbulence. Turbulence was found to be suppressed for  $(d_p/L) < 0.1$ , and augmented for  $(d_p/L) > 0.1$ . Direct Numerical Simulations of particle-laden turbulent flows by Squires & Eaton[2], found that particles are preferentially concentrated in high strain regions, and expelled from high vorticity regions. Elghobashi & Turesdell[3] found that particles increase the turbulent energy at high wave numbers, and suggested a transfer of energy from the large to small scales due to the particles in the absence of gravity, and a reverse cascade from small to large scales in the presence of gravity. Li and McLaughlin[4] reported that particles increase the turbulence intensity at low loading, whereas they suppress the turbulence intensity at high loading. Based on a review of experimental and numerical results, Tanaka & Eaton [5] identified a particle momentum number; they found that particles with small momentum number increase turbulence, whereas those with moderate momentum number decrease turbulence. Recent simulations of Vreman[6] and Capecelatro et al[7] also report that the turbulence intensity progressively decreases with particle loading, as the increased dissipation due to the particles compensates for the decrease in the fluid turbulent energy production.

Here, we critically examine the turbulence attenuation mechanism, specifically whether the decrease in turbulence intensity is continuous as the particle loading is increased, and

whether the excess dissipation due to the particle phase does result in turbulence attenuation. The Reynolds number based on the average flow velocity, channel width and the gas kinematic viscosity is set to a fixed value of 3333. The particle Reynolds number  $Re = (\rho d_p \Delta u / \mu)$  is 42, where  $\rho$  is the fluid density,  $d_p$  is the particle diameter,  $\Delta u$  is the maximum difference in the mean particle and fluid velocities and  $\mu$  is the gas viscosity. The particle Stokes number is the ratio of the viscous relaxation time and the fluid time scale, the latter here considered as  $\tau_f = (h/\bar{u})$ . For the inertia-corrected drag law, equation 1, the viscous relaxation time is  $\tau_v = (\rho_p d_p^2 / 18\mu(1 + 0.15Re^{0.667}))$ . The ratio of the two time scales,  $St = (\tau_v/\tau_f)$  is varied in the range 1.91 – 153.16. The particle volume fraction is varied in the range  $0 - 2 \times 10^{-3}$ , resulting in a variation in the range 0 – 9 for the particle mass loading. The Kolmogorov scale,  $(\nu^3/\epsilon)^{1/4}$ , is about  $1.6 \times 10^{-2}$  times the channel width for the unladen flow, where  $\epsilon$  is the rate of dissipation of energy due to the turbulent fluctuations, and  $\nu = (\mu/\rho)$  is the kinematic viscosity. The particle diameter is comparable to the Kolmogorov scale, so we use the point force approximation for the particles. This also implies that the particles can not directly disrupt the coherent structures in the flow.

The configuration and co-ordinate system used for the simulations is shown in figure 1. The dimensions of the channel are  $4\pi h \times h \times (2\pi h/3)$  in the flow (x), wall-normal (y) and the span-wise (z) directions, where  $h$  is the channel width. Zero velocity boundary conditions are applied at the walls  $y = \pm h/2$ , while periodic boundary conditions are applied at in the flow and the span-wise directions. Spectral DNS is used, where Fourier transforms are used in the stream-wise and span-wise directions which are periodic, and Chebyshev transforms are used in the cross-stream direction with zero velocity boundary conditions. In order to resolve the smallest scales at  $Re = 3333$ , 128 Fourier modes are used in the flow direction, 64 Fourier modes in the span-wise direction and 65 Chebyshev modes in the cross-stream (y) direction.

The particles are considered to be rigid spheres, and the ratio of the particle diameter and the channel width is  $1.84 \times 10^{-2}$ . The particle terminal velocity is  $4 \times 10^{-3}$  smaller than the fluid average velocity, ( $St = 38.3$ ) and so the gravitational force on the particles is negligible compared to the drag force due to the fluid. The particle Reynolds number is too large for the Stokes law to be valid, and so an inertia-corrected drag law [8],

$$\mathbf{F}_I^D = -3\pi\mu d_p(\mathbf{u} - \mathbf{v}_I)(1 + 0.15Re_I^{0.667}), \quad (1)$$

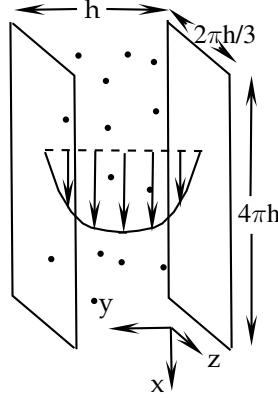


FIG. 1: Configuration and co-ordinate system used for the simulations.

is used. Here,  $\mathbf{F}_I^D$  is the drag force on particle  $I$ ,  $\mathbf{v}_I$  is the particle velocity,  $\mathbf{u}$  is the fluid velocity at the particle location,  $d_p$  is the particle diameter, and  $\text{Re}_I$  is the particle Reynolds number based on the particle diameter, difference in gas and particle velocities  $|\mathbf{u} - \mathbf{v}_I|$  and the gas kinematic viscosity. Equation 1 is accurate to within about 2% for  $\text{Re} = 42$  for an isolated particle in a fluid.

The hard sphere molecular dynamics simulation procedure is used for the particles, where the particle positions are updated based on the particle velocity, and the particle velocity is evolved using Newton's laws. The force on the particle is the sum of the gravitational force (which is negligible in the present case), the drag force (equation 1) and the force due to inter-particle and particle-wall collisions. The inter-particle collisions are modeled using the elastic hard-sphere model, where the relative velocity between a pair of particles along the line joining centers is reversed in a collision, while the relative velocity perpendicular to the line joining centers is unchanged. The particle-wall collisions are considered specular, where the particle velocity perpendicular to the wall is reversed in a collision, while the particle velocity parallel to the wall is unchanged. The force exerted by the particle on the fluid, which is the negative of the drag force, is treated as a delta function force located at the particle center. This approximation is justified because the particle diameter is comparable to the Kolmogorov length scale. This force is included in the Chebyshev-Fourier transformed fluid momentum equations.

The initial condition for the simulation is a steady unladen turbulent flow, where the particles are added at random locations with the same velocity as the fluid velocity. The simulation is run for 3000 integral times to reach steady state, where the integral time is

the ratio of the channel width and the mean fluid velocity. The fluid and particle statistics are then calculated over a period of 1000 integral times. The mean fluid velocity,  $\bar{u}_x$ , is a function of the cross-stream co-ordinate  $y$ . The velocity fluctuations in the flow, cross-stream and span-wise directions are  $u'_x, u'_y$  and  $u'_z$ . The overbars are used to denote time averages, for example the mean square velocity in the flow direction is  $\overline{u'^2_x}$ . The cross-section averaged flow velocity  $\bar{u}$  and the channel width  $h$  in the cross-stream direction are used for non-dimensionalisation.

The effect of particle loading on the mean and the root mean square of the fluctuating velocities are shown in figures 2 for particle Stokes number 38.3. The mean and root mean square velocities are symmetric about the center-line of the channel, and so each quantity is plotted in one half of the figure. The left half of figure 2 (a) shows the variation in mean velocity profiles with particle volume fraction. The mean velocity is close to the turbulent velocity profile for the unladen turbulent flow when the volume fraction is increased from 0 to  $9 \times 10^{-4}$ . There is a distinct change in the velocity profile when the volume fraction is increased from  $9 \times 10^{-4}$  to  $10^{-3}$ . The velocity profile has a lower curvature near the walls and smaller gradient at the walls. When the volume fraction is further increased to  $1.4 \times 10^{-3}$ , there is little change in the velocity profile.

The change in the mean velocity profile is accompanied by a drastic reduction in the mean square velocities in all three directions. The stream-wise mean square velocity in the right half of figure 2 (a) exhibits the characteristic near-wall maximum for a turbulent flow when the volume fraction is  $9 \times 10^{-4}$  or less. When the volume fraction is increased from  $9 \times 10^{-4}$  to  $10^{-3}$ , there is a dramatic collapse in the mean square of the stream-wise fluctuations by one order of magnitude. Upon further increase in the volume fraction, there is very little change in the mean square of the fluctuating velocities.

A dramatic decrease is also observed in the mean square velocities in the wall-normal direction, as shown in the left half of figure 2 (b). More importantly, there is also a virtual collapse in the Reynolds stress as shown in the right half of figure 2 (d). This implies that the suspension stress is primarily due to viscosity and momentum transport by the particles for volume fraction  $10^{-3}$  and above.

The mean square of the particle velocity fluctuations have also been examined. The particle concentration and mean velocity are uniform across the channel, and there is virtually no change in the particle mean velocity as the volume fraction of the particles is increased.

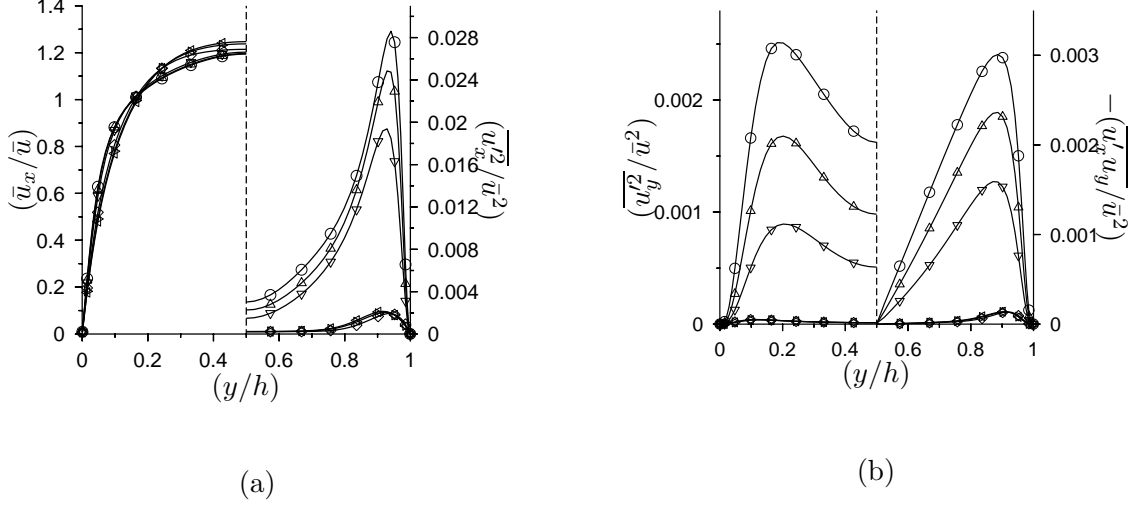


FIG. 2: In sub-figure (a), the fluid mean velocity (left half) and the stream-wise mean square fluctuating velocity (right half), and in sub-figure (b), the cross-stream mean square velocity (left half) and the correlation  $\overline{u_x' u_y'}$  (right half), all suitably scaled by the powers of the average flow velocity  $\bar{u}$ , as a function of the scaled co-ordinate  $(y/h)$ , for average particle volume fraction 0 ( $\circ$ ),  $5 \times 10^{-4}$  ( $\triangle$ ),  $9 \times 10^{-4}$  ( $\nabla$ ),  $10^{-3}$  ( $\triangleleft$ ),  $1.1 \times 10^{-3}$  ( $\triangleright$ ), and  $1.4 \times 10^{-3}$  ( $\diamond$ ). The particle Stokes number is 94.5.

There is a small but discernible increase of about 10-20% in the mean square velocities of the particles, but there is no dramatic change as that observed in the fluid turbulence.

The discontinuous transition in the turbulence intensities is observed for other values of the particle Stokes number, and also if the Stokes drag law is used instead of the inertia-corrected drag law equation 1. This indicates that the discontinuous transition is a robust process independent of the particle Stokes number and the details of the drag law used. The critical volume fraction, is shown as a function of the particle Stokes number in figure 3. For Stokes drag law with inertial correction, critical volume fraction is independent of Stokes number when  $St \geq 40$ , and it appears to increase as the Stokes number decreases for  $St \leq 40$ . Similarly for Stokes drag law, the critical volume fraction increase as the Stokes number decreases when  $St \leq 100$  and then it is constant for  $St \geq 100$ .

In order to examine the mechanism of turbulence attenuation, we have calculated separately the total rate of dissipation of fluid kinetic energy, the rate of dissipation due to the particle drag  $\mathcal{D}_p$ , and the rate of turbulent production of energy  $\mathcal{P}$ . The scaled rate of production of kinetic energy across the channel, which is also the scaled dissipation rate due

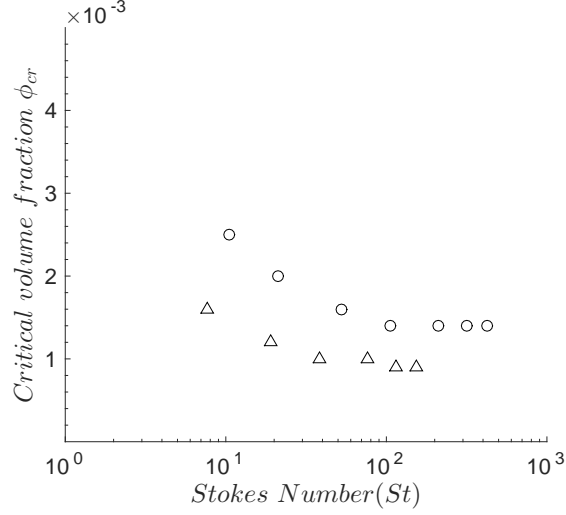


FIG. 3: The critical volume fraction for the turbulence collapse transition as a function of the particle Stokes number ( $St$ ) for the inertia-corrected drag law equation 1 ( $\Delta$ ) and the Stokes drag law ( $\circ$ ).

to the turbulent velocity fluctuations at steady state, is,

$$\mathcal{P} = -\frac{h}{\bar{u}^3} \langle \overline{u'_x u'_y} \frac{d\bar{u}_x}{dy} \rangle_s, \quad (2)$$

where  $\langle \rangle_s$  is the spatial average across the channel. The scaled rate of dissipation of energy due to the mean shear is,

$$\mathcal{D}_f = \frac{\mu}{(\rho \bar{u}^3/h)} \langle \left( \frac{d\bar{u}_x}{dy} \right)^2 \rangle_s. \quad (3)$$

The scaled rate of dissipation of energy due to the drag force exerted by the particles is

$$\mathcal{D}_p = \frac{h}{\rho \bar{u}^3 V} \sum_I \overline{\mathbf{u} \cdot \mathbf{F}_I}, \quad (4)$$

where  $\mathbf{F}_I$  is the force exerted by particle  $I$  on the fluid, and  $V$  is the total volume. The total rate of dissipation of energy per unit mass of gas  $\mathcal{D} = -\mathcal{P} + \mathcal{D}_p + \mathcal{D}_f$ .

The rates of total energy dissipation, turbulent production and dissipation due to the particles are shown as function of the volume fraction for three different values of the particle Stokes number in figure 4. It is observed that there is a significant decrease even in the total rate of dissipation of energy at the critical volume fraction. There is a dramatic collapse in the rate of turbulent production. There is an increase in the rate of dissipation due to the particles, but this increase is only about one half of the decrease in the turbulent

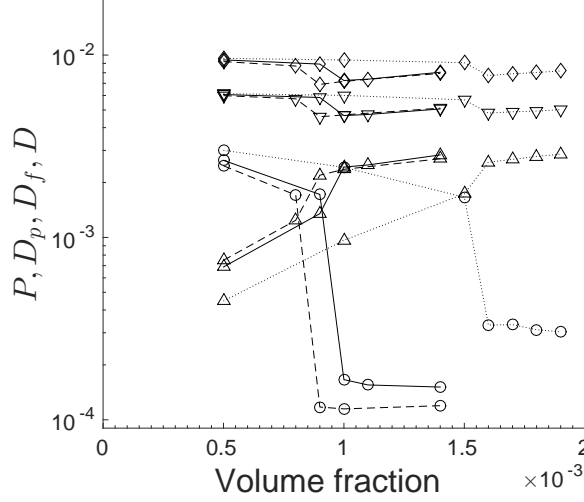


FIG. 4: The scaled total rate of dissipation of energy per unit mass  $\mathcal{D}$  ( $\diamond$ ), the rate of transfer of energy per unit mass from the mean flow to the fluctuations  $\mathcal{P}$  ( $\circ$ ), the rate of dissipation of energy due to the drag force exerted on the particles  $\mathcal{D}_p$  ( $\triangle$ ), and the rate of dissipation of energy due to the mean shear in the fluid  $\mathcal{D}_f$  ( $\nabla$ ) as a function of volume fraction for particle Stokes number 7.66 (dotted lines), 38.3 (solid lines), 114.9 (dashed lines).

production. Thus, turbulence collapse is not accompanied by a compensatory increase in the energy dissipation due to the particle drag, but instead there is a decrease in the total energy dissipation rate. This indicates that the turbulence attenuation is due to a disruption of the turbulence production mechanism, rather than an increase in dissipation due to the particles.

The present study has been limited to a relatively low Reynolds number of about 3333. The other parameters have been varied over relatively wide ranges — two different drag laws have been used, the Stokes drag law and a modification of the Stokes law with inertial correction, equation 1, six different values of the particle Stokes number has been studied for each drag law, about 5-6 particle loadings have been considered for each Stokes number to detect turbulence collapse, and each simulation has been repeated at least 3 times resulting in a comprehensive study involving more than 200 simulations. This study has uncovered a heretofore unknown phenomenon, which is the discontinuous decrease in the turbulence intensity at a critical volume loading in a particle-gas suspension. This is in contrast to the conventional wisdom that there is a gradual decrease in the turbulence intensities as the



particle loading is increased. The mechanism for turbulence modification, the disruption of the turbulence production of energy in the gas phase, is different from the mechanism of increased particle dissipation which was previously considered responsible for turbulence attenuation. In the present case, there is no comparable increase in the dissipation due to the particle fluctuations, and therefore the turbulence attenuation is not due to the increased dissipation by the particles.

The authors thank the SERB, Department of Science and Technology, Government of India, for financial support. VK would like to thank the JRD Tata Trust for supporting this research.

- 
- [1] R. A. Gore and C. T. Crowe. Effect of particle size on modulating turbulent intensity. *Int. J. Multiphase Flow*, 15:279, 1989.
  - [2] K. D. Squires and J. K. Eaton. Preferential concentration of particles by turbulence. *Phys. Fluids A*, 3:1169, 1991.
  - [3] S. Elghobashi and G. C. Truesdell. On the two-way interaction between homogeneous turbulence and the dispersed solid particles 1:turbulence modification. *Phys. Fluids A* 5, 5:1790, 1993.
  - [4] Y. Li and J. B. McLaughlin. Numerical simulation of particle-laden turbulent channel flow. *Phys. Fluids*, 13:2957, 2001.
  - [5] T. Tanaka and J. K. Eaton. Classification of turbulence modification by dispersed spheres using a novel dimensionless number. *Phys. Rev. Lett.*, 101:114502, 2008.
  - [6] AW Vreman. Turbulence attenuation in particle-laden flow in smooth and rough channels. *Journal of Fluid Mechanics*, 773:103–136, 2015.
  - [7] Jesse Capece de Almeida, Olivier Desjardins, and Rodney O Fox. On the transition between turbulence regimes in particle-laden channel flows. *Journal of Fluid Mechanics*, 845:499–519, 2018.
  - [8] Chris D Dritselis. Direct numerical simulation of particle-laden turbulent channel flows with two-and four-way coupling effects: budgets of reynolds stress and streamwise enstrophy. *Fluid Dynamics Research*, 48(1):015507, 2016.